# Multiple scattering of acoustic waves and porous absorbing media

V. Tournat,* V. Pagneux, D. Lafarge, and L. Jaouen
*Laboratoire d'Acoustique de l'Université du Maine, UMR-CNRS 6613, Université du Maine, Av. Olivier Messiaen, 72085 Le Mans cedex 9, France*
(Received 4 February 2004; published 31 August 2004)

Porous media like air-saturated polymer foams with open cells, have a nontrivial frequency-dependent absorption that arises due to viscous and thermal effects at the scale of the rigid frame microstructure. In order to produce multiple scattering at ultrasonic frequencies, mesoscale scatterers are introduced in the porous medium host. The effective wave number of such a multiscale medium should take into account the peculiar absorption at the microscale and the multiple scattering at the mesoscale to describe precisely the propagation of a coherent acoustic wave. For this purpose, a simple model is developed. First, an equivalent fluid model, derived from a homogenization method, is used to describe the acoustic propagation in the host porous medium itself. Second, the scattering by the inclusions is described with a multiple scattering approximation (independent scattering approximation). This simple model allows to obtain the total effective wave number of the porous medium with mesoscale scatterers. After some validating results on the multiple scattering by an array of rigid cylinders in air, experiments on the multiple scattering by rigid cylinders embedded in a porous medium are presented and compared to the developed simple model. Incidentally, it appears that for the host medium itself, the equivalent fluid model is not capable to describe the high-frequency behavior whilst a multiple scattering approach with (thin) viscous and thermal boundary layers around the scatterers is accurate in the whole frequency range.

DOI: 10.1103/PhysRevE.70.026609 PACS number(s): 43.20.+g, 43.35.+d

The multiple scattering of classical waves in inhomogeneous media has been extensively studied these past 50 years [1–7]. For elastic waves, weakly dissipative host media for scatterers are often used: water, solid plates [8–10]. However, in the case of host media like porous absorbing materials implying a strong dissipation, the nontrivial frequency dependent absorption that arises in such media has to be taken into account to describe the acoustic wave propagation. For acoustic porous materials, at long wavelength $\lambda$, i.e., when the latter is much larger than the characteristic dimension of the microstructure (the microscopic scale), the propagation is well described by the homogenized theory of porous materials [11–21], which is analogous in some respects to the theory of electromagnetic wave propagation in dielectric materials [22]. If we introduce scatterers with a mesoscopic scale much larger than the microscopic scale in the porous medium, the propagation can be described by a multiscale approach; the multiple scattering by the scatterers at the mesoscale can be described by a multiple scattering approximation and takes place in a homogenized porous absorbing medium described by the above mentioned homogenized theory of porous materials. This regime, where dissipation and scattering take place, has not been extensively studied. Paradoxically, this latter is of real interest due to the numerous opportunities to meet such a problem, e.g., in biological ultrasonics [23] and in seismics [24].

In this paper, we want to investigate the effective medium properties when both multiple scattering and absorption effects are present. Concerning multiple scattering, several effective medium approximations have been proposed in the literature [5]. Since our experiments are concerned with sparse distributions of scatterers, we have chosen the so-called independent scattering approximation (ISA) [25], theoretically valid for low densities of randomly located scatterers. This approximation only requires the scattering amplitude of one scatterer in the forward direction and the density of scatterers in the medium. Concerning the absorption, it is taken into account by considering viscous and thermal effects at the microscopic scale.

In the first part, we present results from experiments at ultrasonic frequencies in a random array of rigid cylinders placed parallel in air. In this case, viscous and thermal effects occur mainly in the boundary layers at the cylinder surface. When these effects are taken into account in the ISA, it yields a modified ISA (ISA$\beta$) with a small correction to the effective wave number. Measurements of the coherent wave attenuation and velocity are compared to the theory. This validates the chosen multiple scattering approximation for a filling ratio up to 0.1 and for wavelengths ranging from 40 to 4 cylinder radius.

In the second part, the random array of rigid parallel cylinders is embedded in a porous material—an air-saturated polyurethane foam with open cells and low flow resistivity. According to the homogenized theory, as long as the wavelength is large compared to the characteristic microscale, this latter material can be considered as an equivalent fluid possessing nontrivial frequency dependent absorption. Then, the effect of the rigid cylinders on the coherent wave propagation can be taken into account using the ISA with the equivalent fluid as the host medium. Comparisons of this simple multiscale approach with measurements for two different filling ratios of rigid cylinders are done. Results show that the presence of scatterers has a significant effect on both the

*Electronic address: vincent.tournat@univ-lemans.fr

 

attenuation and phase velocity of the coherent wave. For the highest frequencies, as confirmed by the experimental results, the equivalent fluid idealization of the host porous medium is no longer completely valid and additional scattering effects by the microstructure manifest themselves. It appears that these effects may be taken into account in the present multiscale description, by modeling the host medium with an *ad hoc* utilization of ISA$\beta$. The resulting description enables us to accurately match the experimental data in the whole frequency range, taking into account both aspects of absorption and scattering.

## I. PRELIMINARY EXPERIMENTS AND MULTIPLE SCATTERING APPROXIMATION ANALYSIS

A quantity that is of interest for the propagation of an acoustic wave in a multiple scattering medium is the configurationally averaged Green's function, related to the propagation of the coherent amplitude [5]. This function can be written as

$$\langle G\rangle(\omega,\vec{k}) = \frac{1}{k_0^2(\omega) - k^2 - \Sigma(\omega,\vec{k})}, \tag{1}$$

where $\langle\cdots\rangle$ denotes the configurational average, $k_0$ is the uniform-medium wave number, $\omega$ the angular frequency, $\vec{k}$ the wave vector, and $\Sigma(\omega,\vec{k})$ is the self-energy.

The self-energy $\Sigma(\omega,\vec{k})$ that arises because of the local deviations of the medium wave number from the uniform-medium value $k_0$, contains information about the multiple scattering. In particular, if in a regime, the self-energy has no $\vec{k}$ dependence, it becomes possible to define an effective medium, seen as a homogeneous medium by the coherent amplitude [5]. Owing to Eq. (1), the propagation of the coherent amplitude is described by an effective wave number $k_e$ such that

$$k_e^2 = k_0^2 - \Sigma(\omega) \tag{2}$$

and the problem is reduced to determining the complex self-energy.

The independent scattering approximation assumes that there is no correlation between the scatterers [6]. In this approximation, the self-energy, the quantity which is used to renormalize the effective wave number of the multiple scattering medium, is expressed by [25]

$$\Sigma(\omega) = n\langle\vec{k}_0|t|\vec{k}_0\rangle, \tag{3}$$

where $n$ is the density of scatterers in the medium, and $\langle\vec{k}_0|t|\vec{k}_0\rangle$ the term of forward scattering of the $t$- matrix for a single scatterer. In this section, we consider a random array of rigid cylinders placed parallel in the air and we apply the above theory. The governing equation of the host medium (air) is the Helmholtz equation and two different boundary conditions on the cylinder are considered in the model: (i) Neumann boundary condition without absorption; (ii) impedance boundary condition with absorption.

In the case of a plane wave incident on a two-dimensional (2D) cylindrical scatterer at rest, the acoustic pressure can be written

$$p(r,\theta) = \sum_{m=0}^{+\infty} p_m = \sum_{m=0}^{+\infty} i^m(2-\delta_{m0})[J_m(k_0r) + D_mH_m(k_0r)]\cos(m\theta), \tag{4}$$

where $D_m$ are the scattering coefficients. Expressing the self-energy $\Sigma(\omega)$ in terms of the scattering coefficients $D_m$, it yields [26]

$$\Sigma(\omega) = 4ni\sum_{m=0}^{+\infty}(2-\delta_{m0})D_m. \tag{5}$$

Without absorption, the classical Neumann boundary conditions for rigid scatterers are used, and the scattering coefficients are given by

$$D_m = -\frac{J_m'(k_0R)}{H_m'(k_0R)}, \tag{6}$$

where $R$ is the cylinder radius, and $J_m'$ and $H_m'$ are the first derivatives of the cylindrical Bessel and Hankel functions.

With absorption, the equivalent surface admittance can be used to take into account the viscous and thermal effects which occur in the boundary layers and are generally neglected out. New scattering coefficients $D_m$ including these effects are obtained as follows. In the case of a plane wave incident on a motionless flat surface of large heat capacity, the equivalent surface admittance $\beta$ relates the pressure and the normal derivative of the pressure by $-i\beta k_0 p = \partial p/\partial n$ and has the following form [26] (convention $e^{-i\omega t}$):

$$\beta = \frac{1-i}{2}k_0\left[(\gamma-1)\delta_h + \left(1-\frac{k_{0\perp}^2}{k_0^2}\right)\delta_v\right], \tag{7}$$

where $\gamma$ is the air specific heat ratio, $\delta_h$ the thermal boundary layer thickness, $\delta_v$ the viscous boundary layer thickness, and $k_{0\perp}$ the normal component of the air wave vector. Assuming that the scatterer is cylindrical, rigid, and of large heat capacity, an expression for the admittance $\beta_m$ seen by a component $m$ of the field in Eq. (5) can be obtained by identifying in Eq. (7) the normal wave number $k_{0\perp}$ with the radial wave number $k_r$. Since $k_r^2 = k_0^2 - m^2/r^2$, the following admittance is obtained:

$$\beta_m = \frac{1-i}{2}k_0\left[(\gamma-1)\delta_h + \frac{m^2}{k_0^2R^2}\delta_v\right]. \tag{8}$$

The condition to use this admittance $\beta_m$ is that the surface should appear locally flat, i.e., $\delta_h$ and $\delta_v \ll R$. Applying the mixed boundary conditions at $r=R$,

$$-i\beta_m k_0 p_m = \frac{\partial p_m}{\partial r}, \tag{9}$$

it is possible to determine the scattering coefficients:

$$D_m = -\frac{J_m'(k_0R) + i\beta_m J_m(k_0R)}{H_m'(k_0R) + i\beta_m H_m(k_0R)}. \tag{10}$$

The use of these new coefficients in the previous ISA formula, Eq. (5), takes into account the viscous and thermal losses at the boundaries of the scatterers. In the following, ISA$\beta$ will denote this modified ISA.

Using Eqs. (5) and (2), the effective wave number $k_e$ can be explicitly evaluated. Eventually, the phase velocity $v$ of the coherent wave is

$$v = \frac{\omega}{Re(k_e)}, \tag{11}$$

and the transmission coefficient $A$ by a slab of thickness $L$, neglecting the reflections at the slab interfaces is

$$A = e^{-Im(k_e)L}. \tag{12}$$

### A. Long-wavelength limit

The physical consistency of the present multiple scattering approach ISA$\beta$ may be checked in a nontrivial manner in the long-wavelength limit $k_0R \to 0$, by comparison with the known high-frequency limit of the homogenized method, described in Appendix A and denoted as the equivalent fluid model (EFM) [20].

On the one hand, when the wavelength becomes very large compared to the cylinder radius, Rayleigh scattering occurs (monopole and dipole radiation). The self-energy summation (5) may be limited to $m=0,1$, and the Bessel and Hankel functions in Eq. (10) may be developed using known expansions. To the leading order in $k_0R$ the result is

$$k_e^2 = k_0^2\left\{1 + f\left[1 + (1+i)\left(\frac{2\delta_v}{R} + (\gamma-1)\frac{\delta_h}{R}\right)\right]\right\}, \tag{13}$$

where the filling ratio $f = n\pi R^2$ is defined as the specific volume of solid cylinders.

On the other hand, the EFM description may be applied to the same problem, assuming that the wavelength is much larger than a "coarse graining" characteristic cell size, which smoothes out the microstructure. Then assuming in addition that the frequency may be taken sufficiently high, so that the boundary layers appear locally plane ($\delta_v, \delta_h \ll R$), the EFM results can be expanded in powers of the viscous and thermal skin depths and an exact asymptotic expansion can be written for $k_e^2$ [15,20,21,29]:

$$k_e^2 = k_0^2\ \alpha_\infty\left[1 + (1+i)\left(\frac{\delta_v}{\Lambda} + (\gamma-1)\frac{\delta_h}{\Lambda'}\right)\right], \tag{14}$$

where $\alpha_\infty$, $\Lambda$, and $\Lambda'$ are three independent geometrical parameters, described in Appendix A. To compare this result with that of the ISA$\beta$, Eq. (13), we note that the latter is thought to be exact only in a corresponding dilute limit. This is because the effect of the correlations between the scatterers, not included in the ISA$\beta$, will affect the higher order terms that cannot be discarded when the concentration increases. For our check of consistency, a dilute approximation is thus to be introduced in Eq. (14). For dilute arrays of parallel cylinders and a propagation normal to the cylinders, the following are exact results, to the first order in the filling ratio $f$ [27]:

$$\alpha_\infty = 1 + f, \quad \frac{1}{\Lambda} = \frac{2f}{R}, \quad \frac{1}{\Lambda'} = \frac{f}{R}. \tag{15}$$

Thus it is verified that, to the first order in volume fraction $f$, the low frequency limit of the multiple scattering approach (ISA$\beta$) and the high frequency limit of the homogenization approach (EFM) are the same.

### B. Experiments

The sample consists of a disordered arrangement of parallel rigid cylinders embedded in air. The disorder is obtained by building a roughly regular array of parallel cylinders. The cylinder radius is 0.4 mm and the filling ratio is $f \simeq 0.1$. For the ultrasonic excitation and detection, the same wide bandwidth (20–200 kHz) transducers are used. The signal to noise ratio is improved by repetitive averaging of the detected signals using a digital oscilloscope. A rough estimation of the separations between cylinders is about 2 mm, which is not small compared to the wavelength (17–1.7 mm). Thus it is known *a priori* that the long-wavelength theory (EFM) will not be capable to describe the propagation.

An interesting quantity to plot is the transmission coefficient of the coherent amplitude through the slab sample [see Eq. (12)]. The coherent acoustic amplitude, which propagates in the sample as in an effective homogeneous medium, is obtained experimentally by averaging the transmitted pulse over 40 positions of the sample [8]. Notice also that the diameter of the transducer (4 cm) is not small compared to the wavelengths (17–1.7 mm), and this corresponds to an additional averaging. However, it remains a part of incoherent field in the averaged signal, which causes fluctuations in the results of the experimental transmission coefficient and the phase velocity. As the discontinuity of impedance at the sample surfaces has a very weak effect on the transmitted coherent amplitude for this filling ratio, the back propagating waves in and out the sample are neglected. The transmission coefficient is then supposed to be the attenuation of the coherent amplitude over the thickness of the sample [20]. In Fig. 1, the experimental transmission coefficient is plotted versus frequency, from 30 to 180 kHz, and compared to the estimation of the ISA and the ISA$\beta$ [Eqs. (2), (5), (6), and (12) and Eqs. (2), (5), (10), and (12), respectively]. Notice that the ratio $\delta_{h,v}/R$ varies in this frequency range from 1/25 to 1/80, thus ensuring the validity of the relation (8).

For both the transmission coefficient and the phase velocity of the coherent amplitude, plotted in Fig. 2, the ISA and the ISA$\beta$ fit the experimental data. The correction included in the ISA$\beta$ which takes into account the effect of the viscous and thermal boundary layers is too weak compared to the noise of the experimental data to allow direct validation. However, a slight improvement is observed in the low frequency range for both transmission coefficient and phase velocity measurements.

The lower values obtained by the ISA$\beta$ are due to the viscous and thermal losses. As can be expected, the difference between the two models is more important in the low frequencies because of the larger extent of the viscous and

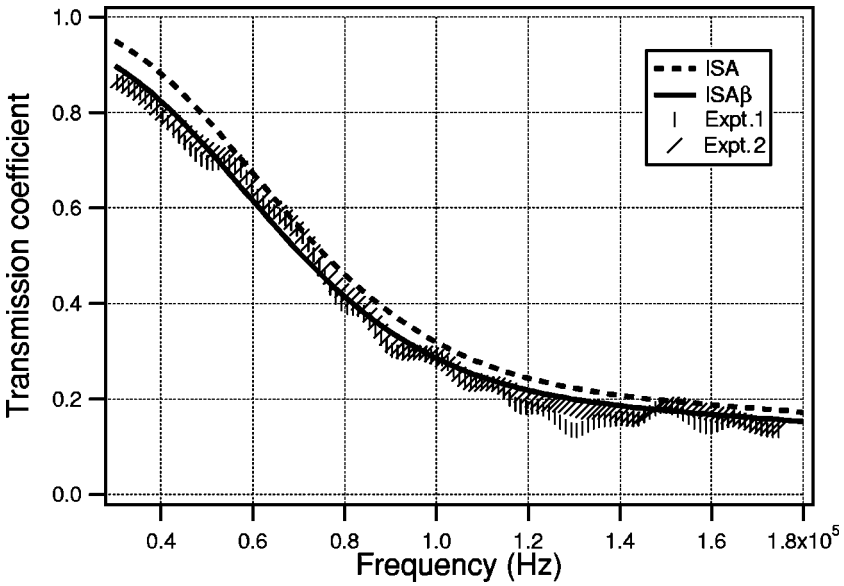


FIG. 1. Transmission coefficient of the coherent amplitude through the slab of thickness 2 cm, composed of parallel rigid cylinders of radius 0.4 mm with a filling ratio of $f \simeq 0.1$. Experimental curves (Expt. 1 and Expt. 2) are obtained with two different couples of transducers.

thermal boundary layers. We note that the satisfactory agreement between experimental data and ISA$\beta$ justifies the use of the independent scattering approximation, up to filling ratios on the order of $f=0.1$. The ISA will be used next in the similar problems with an equivalent fluid porous medium replacing the air, and different kind of scatterers.

## II. MULTIPLE SCATTERING IN POROUS ABSORBING MEDIA

In this section, the problem of the propagation of acoustic waves in a multiple scattering and absorbing porous medium is treated (see Fig. 3). We consider a host fluid material *A*—generally an equivalent fluid porous material—in which scatterers *B*—fluid, equivalent fluid, or rigid—have been immersed randomly and with a low density (less than 10% of the total volume typically).

First, the different cases are treated analytically by the multiscale approach, with scatterers given by parallel cylinders (2D problem) or spheres (3D problem). Second, experimental results for the attenuation and velocity of a coherent wave in slabs of rigid cylinders placed parallel in a polymer foam are presented and compared to the developed multiscale approach.

### A. Multiple scattering description

According to the equivalent fluid model, the long-wavelength sound propagation in a rigid frame porous material is formally the same as in a fluid with complex, frequency-dependent, density $\rho(\omega)$ and bulk modulus $K(\omega)$. The precise definition and modeling of these effective quantities is recalled in Appendix A. From the effective density and bulk modulus, it is possible to determine the equivalent fluid wave number $k(\omega)=\omega/\sqrt{K(\omega)/\rho(\omega)}$ and characteristic impedance $Z(\omega)=\sqrt{\rho(\omega)K(\omega)}$.

In the following, subscripts *A*, *B* will be used to distinguish the quantities related to the host and scatterer materials

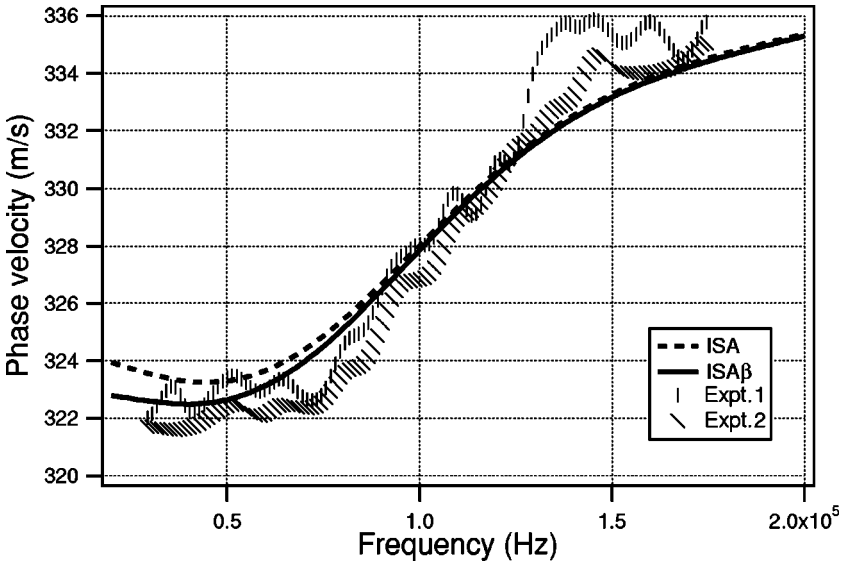


FIG. 2. Phase velocity of the coherent amplitude in the slab composed of parallel rigid cylinders of radius 0.4 mm with a filling ratio of $f \simeq 0.1$. Experimental curves (Expt. 1 and Expt. 2) are obtained with two different couples of transducers.

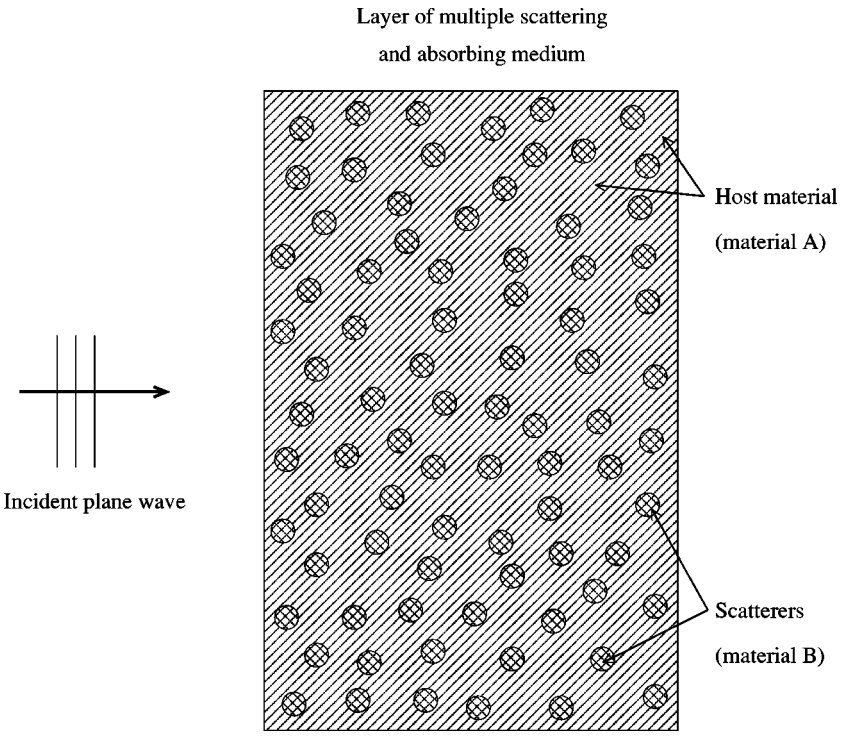


FIG. 3. Problem under consideration.

*A*, *B*. The expression of the scattering coefficients Eq. (6), now need to be generalized by taking into account the propagation in material *B* and the appropriate boundary conditions at the interface between material *A* and *B*. As discussed in Appendix A, the usual continuity conditions of pressure and normal velocity still apply, with appropriate definition of the "macroscopic" pressure and velocity. Thus, in the 2D problem, the scattering coefficients are given by (see Appendix B)

$$D_m = \frac{\frac{Z_A}{Z_B} J_m(k_A R) J'_m(k_B R) - J'_m(k_A R) J_m(k_B R)}{H'_m(k_A R) J_m(k_B R) - \frac{Z_A}{Z_B} H_m(k_A R) J'_m(k_B R)}. \quad (16)$$

In the 3D problem, the scattering coefficients are (see Appendix B)

$$d_m = \frac{\frac{Z_A}{Z_B} j_m(k_A R) j'_m(k_B R) - j'_m(k_A R) j_m(k_B R)}{h'_m(k_A R) j_m(k_B R) - \frac{Z_A}{Z_B} h_m(k_A R) j'_m(k_B R)}. \quad (17)$$

Then considering a medium with a random distribution of scatterers the self-energy is, in the frame of the independent scattering approximation [5,25],

$$\Sigma_{2D}(\omega) = 4ni \sum_{m=0}^{+\infty} (2 - \delta_{m0}) D_m \quad (18)$$

and

$$\Sigma_{3D}(\omega) = \frac{4\pi ni}{k_A} \sum_{m=0}^{+\infty} (2m+1) d_m. \quad (19)$$

Using Eqs. (18) and (19), the effective wave number of the multiple scattering and absorbing medium is then determined in the 2D or 3D case as

$$k_e = [k_A^2 - \Sigma_{2D}(\omega)]^{1/2} \quad (20)$$

or

$$k_e = [k_A^2 - \Sigma_{3D}(\omega)]^{1/2}. \quad (21)$$

These results can be directly applied to different problems: fluid scatterers (like holes filled with air) in a porous medium, porous scatterers in a fluid medium, and porous scatterers in a different porous matrix. For the case of rigid scatterers embedded in a porous medium, one must consider that the characteristic impedance ratio $Z_A/Z_B$ vanishes and use the simplified expressions (B9) and (B10) of the scattering coefficients.

### B. Experiments

Without resonant scattering, strongest effects of the multiple scattering in a porous medium are obtained with rigid scatterers due to the "infinite" impedance mismatch between the scatterers and the matrix host material. Besides, resonant scattering is difficult to achieve due to the low quality factor of porous absorbing media. For these reasons, rigid scatterers have been chosen.

#### *1. Samples and experimental setup*

Samples are polymer foam slabs of 5 cm thickness in which full metallic cylinders (1.6 mm in diameter) have been

TABLE I. Polymer foam parameters used for the computation of the equivalent fluid model.

| $\alpha_\infty$ | $\phi$ | $\Lambda(\mu\text{m})$ | $\Lambda'(\mu\text{m})$ | $k_0(\text{m}^2)$ | $k_0'(\text{m}^2)$ |
|---|---|---|---|---|---|
| 1.053 | 0.98 | 450 | 1000 | $1.88\times10^{-8}$ | $4\times10^{-8}$ |

embedded in a parallel manner but with disordered locations. Values of the characteristic parameters of the polymer foam taking place in the EFM (see Appendix A) are collected in Table I. These parameters have been obtained by other physical or low-frequency acoustical methods and slightly optimized numerically (in the range of their uncertainties) to ensure the best fit with experiments. Two different samples are used (denoted by sample 1 and sample 2) corresponding to two different filling ratios of scatterers, $f_1 \simeq 0.052$ and $f_2 \simeq 0.024$, respectively, or equivalently to the following scatterers densities: $n_1 \simeq 26000\ \text{m}^{-2}$ and $n_2 \simeq 12000\ \text{m}^{-2}$.

The experimental setup is identical to the one of Sec. I B. However, the additional spatial averaging, by translating laterally the samples, has not been performed. A reference signal associated to the acoustic propagation between the ultrasonic emitter and receiver ($\sim$20 cm) in the air only is first registered. Then, the same signal is sent to a slab made of the porous material without the scatterers, placed between the transducers. The received signal spectrum is used to determine the velocity dispersion curve and the transmission coefficient of the slab. Finally, the sample slab made of the porous material with the embedded rigid cylinders is substituted to the previous sample. The associated velocity dispersion and transmission curves are thus obtained.

#### *2. Experimental results and additional modeling*

The transmission coefficient and velocity dispersion curve for the sample 1 ($f_1 \simeq 0.052$) are plotted in Figs. 4 and 5. There exists a strong influence of the scatterers on both phase velocity and transmission coefficient. It is especially the case in the low-frequency part for the velocity plots and in the intermediate frequencies for the transmission coefficient. At low frequency, the four plotted models which are to be next detailed fit correctly the experiments.

Due to the ultrasonic transducers low efficiency under 20 kHz and above 180 kHz, experimental data outside the range 20–180 kHz are noisy.

The dashed thin line corresponds to the equivalent fluid model (EFM) applied to the only porous material, using the parameters of Table I and formulas Eqs. (A4) and (A5) to determine the equivalent wave number. It is obvious that for frequencies higher than $\sim$100 kHz, this model does not describe correctly the propagation in the porous material, the transmission coefficient being overestimated. Indeed, at these frequencies, the acoustic wavelength ($\sim$3 mm and less) becomes comparable to the characteristic size of the micro-structure, i.e., the size of the pores 1–2 mm. It is known *a priori* that the EFM will not be capable to describe this regime where scattering by the microstructure of the porous material itself takes place.

For the low frequency part of the frequency band (20–100 kHz) where scattering by the porous material itself does not play an important role, the immersion of the cylindrical rigid scatterers strongly decrease both the transmission and the phase velocity of the coherent wave in the medium (Figs. 4 and 5). This behavior is well described by the analytical approach developed in this paper for rigid parallel cylinders in a porous medium, i.e., with the help of Eqs. (18) and (20) (where the host medium $A$ is the EFM medium of Table I) and Eq. (B9), for $R=0.4$ mm and $n_1=26000\ \text{m}^{-2}$ (it is important to notice that $R$ and $n_1$ are directly measured quantities and were not adjusted). This approach is plotted in dashed thick lines and is denoted by the EFM+ISA theory.

The same analysis can be done for the experiments performed with the sample 2 ($f_2 \simeq 0.025$) that are plotted in Figs. 6 and 7. The filling ratio $f_2$ of sample 2 being less than the filling ratio $f_1$ of sample 1, the effect of multiple scattering by the rigid cylinders has a weaker effect on the transmission by the slab and on the phase velocity. Once again, due to the scattering by the porous material microstructure

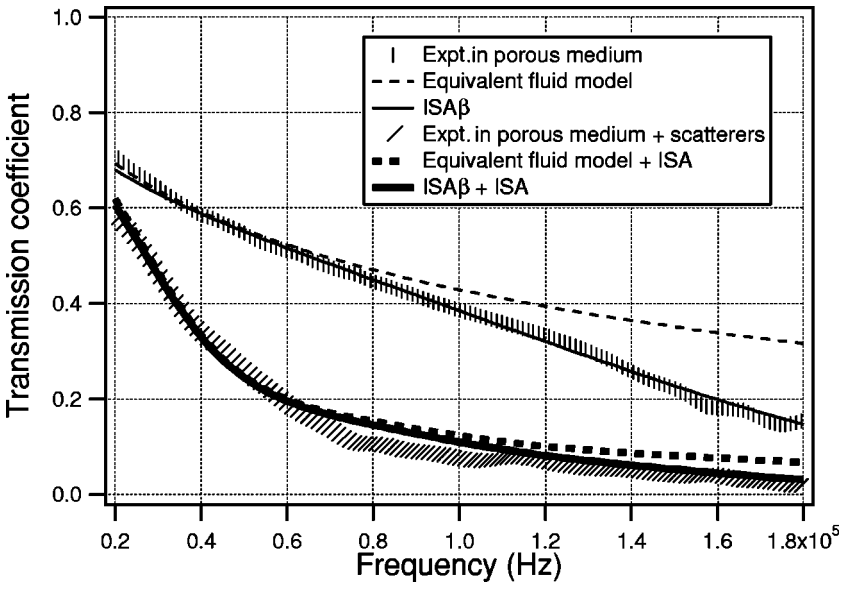


FIG. 4. Transmission coefficient of the sample 1 made of a porous material where parallel rigid cylinders of radius $R=0.8$ mm have been included with the filling ratio $f \simeq 0.052$.

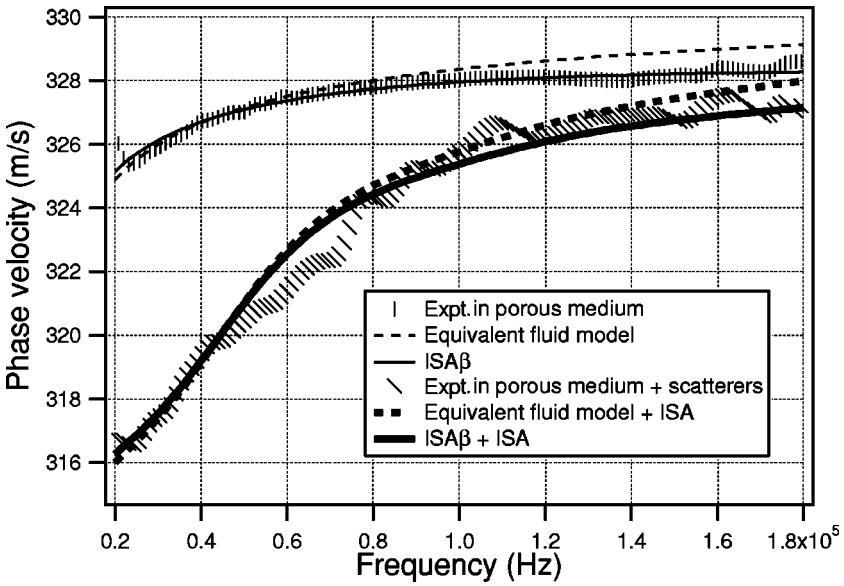


FIG. 5. Phase velocity of the coherent amplitude in the sample 1 made of a porous material where parallel rigid cylinders of radius $R=0.8$ mm have been included with the filling ratio $f \simeq 0.052$.

itself, the EFM does not fit correctly the experimental curves in the high frequency part of the band. In the low frequency part of the band, the associated EFM+ISA theory (with $n_2 \simeq 12\,000\ \mathrm{m}^{-2}$) fits perfectly the experimental deviations from the values of the porous medium due to the presence of the rigid cylinders.

For frequencies low enough that the wavelengths are large compared to the intercylinder distance, the samples with embedded cylinders can be presumably well described by the EFM theory, but with renormalized values of $\alpha_\infty, \Lambda, \Lambda'$. However, in our experimental configuration for which the acoustic wavelengths are less than 3 mm, this could only be checked at much lower frequencies than those presented here, because the intercylinder characteristic distance is estimated to be more than 3 mm.

In order to take into account the scattering that occurs in the porous medium itself above approximately 100 kHz, it appears that an *ad hoc* utilization of ISA$\beta$ is possible.

Exact computation of ISA$\beta$ can be achieved when scatterers are identical and with well defined shapes. However, in the case of polyurethane foams, scatterers are not easily identified, and it is complicated to know *a priori* their characteristic size and density. We have found that it is possible to obtain with the ISA$\beta$ the effective wave number of such media, by searching two equivalent parameters, a scatterer radius $R$ and a scatterer density $n$. A minimization method between experiments and ISA$\beta$ theory has been applied for the imaginary part of the polymer foam wave number, and gives $R \simeq 7.3 \times 10^{-5}$ m and $n \simeq 4.2 \times 10^{6}\ \mathrm{m}^{-2}$.

This ISA$\beta$, applied to the porous medium itself, is plotted in Figs. 4–7 in a continuous thin line. Agreement between experiments and ISA$\beta$ is observed for the whole frequency range. Then it is possible to substitute this ISA$\beta$ new effective wave number as the matrix wave number in the ISA, in order to describe the scattering by the additional mesoscale scatterers. Especially for the transmission coefficient of the sample 2 in Fig. 6, this last modification improves greatly the matching between theory and experiments at high frequencies, when scattering from both the porous medium itself and from the imbedded rigid cylinders is strong.

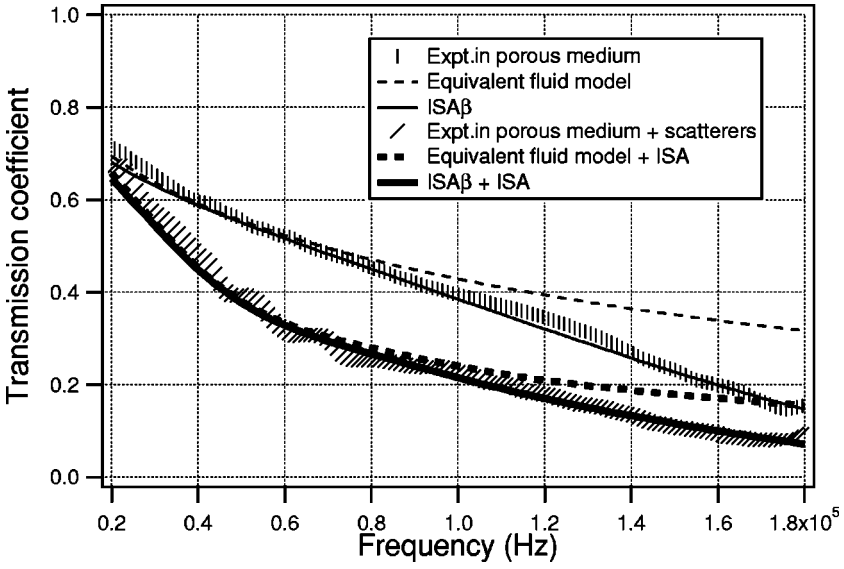


FIG. 6. Transmission coefficient of the sample 2 made of a porous material where parallel rigid cylinders of radius $R=0.8$ mm have been included with the filling ratio $f \simeq 0.024$.

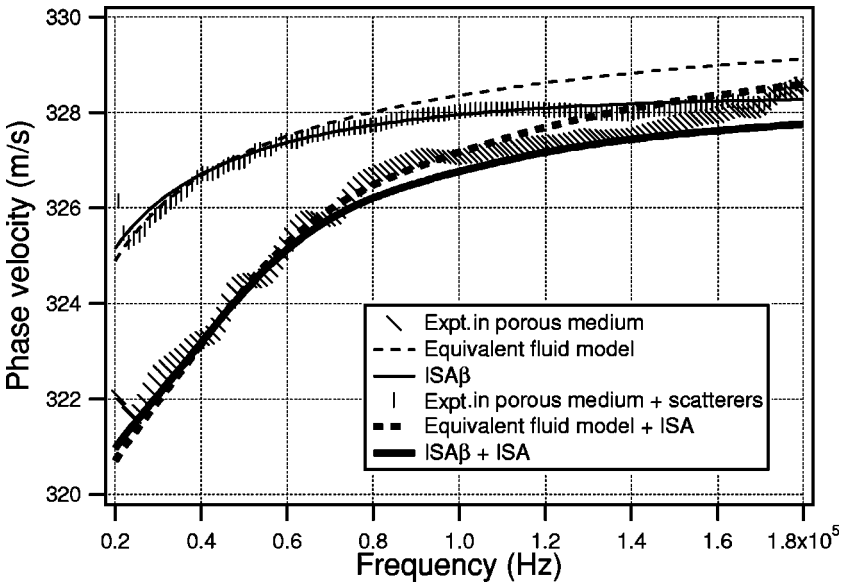


FIG. 7. Phase velocity of the coherent amplitude in the sample 2 made of a porous material where parallel rigid cylinders of radius $R=0.8$ mm have been included with the filling ratio $f \simeq 0.024$.

For higher densities of scatterers, the independent scattering approximation may fail to describe the effective properties of the porous samples and other effective medium theories should be implemented, like, for instance, in Refs. [24,30].

## III. CONCLUSIONS

Modeling of multiple scattering of acoustic waves in porous media, including absorption, is performed in two different problems. In the first one (Sec. I), the microstructure of the medium is made of scatterers with well defined shapes (parallel rigid cylinders). The absorption is included in the ISA through a concept of equivalent surface admittance to take into account viscous and thermal effects. Associated experiment is performed and agrees well with the ISA.

In the second problem (Sec. II), the microstructure of the porous medium is complicated and cannot be described easily with a multiple scattering approximation. The EFM is used to describe the acoustic propagation in the host material and the ISA to take into account the multiple scattering by the included mesoscale scatterers (EFM+ISA model). Experiments have been performed with a porous medium (a polymer foam) in which rigid parallel cylinders have been immersed randomly. In the frequency range 20–100 kHz, the developed model agrees well with the experiments. Above ~100 kHz, scattering by the microstructure of the host porous material itself influences the acoustic propagation. This effect is taken into account by an *ad hoc* utilization of ISA$\beta$ where an equivalent radius and an equivalent density can be found. The obtained host wave number allows us to describe precisely the propagation (including scattering and absorption) in the porous medium itself in the whole frequency range of the experiment. Finally, this wave number is substituted into the description of the acoustic propagation through the medium with additional mesoscale scatterers (ISA$\beta$+ISA), which also improves the agreement with experiments in the whole frequency band 20–180 kHz.

Using this approach, it is possible to account at the same time for the strong dissipation at the microscopic scale and for the multiple scattering at the mesoscopic scale. The so-called "high frequency" limit [20] of the homogenized theory approach for both micro and meso scales is only a particular case of the developed approach, corresponding to a limited frequency band which is both "low frequency" in the sense of scattering effects (wavelength much greater than the characteristic micro and meso scales) and high frequency in the sense of dissipation effects (small viscous and thermal boundary layer thickness at the microscale).

## APPENDIX A: EQUIVALENT FLUID MODEL FOR ACOUSTIC PROPAGATION IN POROUS MEDIA

Let $L$ be a typical averaging length of the microstructure of a rigid frame, air-saturated, porous material, such that this material appears homogeneous (and isotropic) at this scale $L$. When considering (in the framework of linear acoustics) wavelength verifying the long wavelength condition $\lambda \gg L$, it can be shown by spatial averaging methods that an effective wave number appears, such that

$$k_e^2 = k_0^2 \frac{\rho_e/\rho_0}{K_e/K_a}, \tag{A1}$$

where $\rho_e$ is a complex effective density of the air determined by inertial and viscous interactions, and $K_e$ is a complex effective bulk modulus of air determined by thermal exchanges ($K_a$ is the adiabatic bulk modulus). Indeed, it can be shown that in harmonic regime $e^{-i\omega t}$, the two first order macroscopic linear equations for wave propagation are

$$-i\omega\rho_e(\omega)\vec{v} = -\vec{\nabla} p, \tag{A2}$$

$$-i\omega \frac{1}{K_e(\omega)} p = -\vec{\nabla}\cdot\vec{v}, \tag{A3}$$

where $\vec{v}$ and $p$ are the macroscopic velocity and pressure obtained by microscopically averaging the corresponding

fields in the fluid. Equation (A2) is an effective Euler equation, which takes into account the inertial and viscous interactions between solid and fluid. Equation (A3) is an effective equation of state which takes into account the thermal exchanges between solid and fluid. At the open boundary between the equivalent fluid material and the air, the continuity of the normal stress and normal flow will apply. The two continuity conditions reduce to the usual *pressure and normal velocity continuity conditions*, provided the macroscopic variables are conveniently defined: the pressure is defined as an "*air phase average*" and the velocity is defined as a "*total volume average*" (=$\phi\times$ *air phase average*, where $\phi$ is the porosity).

Simple and relatively accurate scaling functions describe the frequency dependence of $\rho_e$ and $K_e$, knowing a finite set of geometrical parameters ($\phi$, $\alpha_\infty$, $k_0$, $\Lambda$, $k_0'$, $\Lambda'$) associated with the porous space. These functions have, in the general case, the following forms [15,19]:

$$\rho_e(\omega) = \frac{\rho_0 \alpha_\infty}{\phi}\left(1 - \frac{1}{ix}\sqrt{1 - \frac{M}{2}ix}\right), \tag{A4}$$

$$K_e(\omega) = \frac{K_a}{\phi}\left[\gamma - (\gamma - 1)\left(1 - \frac{1}{ix'}\sqrt{1 - \frac{M'}{2}ix'}\right)^{-1}\right]^{-1}, \tag{A5}$$

with the following notations:

$$M = \frac{8k_0\alpha_\infty}{\phi\Lambda^2}, \quad M' = \frac{8k_0'\alpha_\infty}{\phi\Lambda'^2},$$

$$x = \frac{\omega\alpha_\infty\rho_0 k_0}{\eta\phi}, \quad x' = \frac{\omega\rho_0 k_0'\mathrm{Pr}}{\eta\phi}.$$

Here, $\phi$ is the porosity (ratio of the fluid volume to the total volume), $\alpha_\infty$ is the Johnson, Koplik, and Dashen tortuosity factor [15], $k_0$, not to be confused with the air wave number, is Darcy's viscous permeability, $\Lambda$ is the Johnson, Koplik, and Schwartz pore size parameter [21,28], $k_0'$ is the Lafarge *et al.* thermal permeability [19], and $\Lambda'$ is the Champoux and Allard pore size parameter [29]. Thermodynamic properties of the saturating fluid—air—are given by $\rho_0$ the ambient density, $K_a$ the adiabatic bulk modulus, $\gamma$ the specific heat ratio, $\eta$ the dynamic viscosity, and Pr the Prandtl number. In acoustics, it is customary to use the air flow resistivity $\sigma = \eta/k_0$, in place of the permeability. This parameter is directly measurable by means of dc air flow resistance measurements.

## APPENDIX B: DERIVATION OF THE SCATTERING COEFFICIENTS FOR POROUS SCATTERERS IN POROUS MEDIA

In order to derive the scattering coefficients of simple shape scatterers, it is convenient to express the acoustic pressure field in the appropriate coordinate system, cylindrical for the 2D problem of cylindrical scatterers, and spherical for the 3D problem of spherical scatterers. As in Sec. II A, we denote by corresponding subscripts $A$ and $B$ the quantities related to the host and scatterer materials.

### 1. 2D problem of cylindrical scatterers

The acoustic pressure field outside the scatterer is written as a function of the distance $r$ to the scatterer's center and the angle $\theta$ between the incident plane wave direction and the observation direction:

$$p_A(r,\theta) = \sum_{m=0}^{+\infty} i^m(2 - \delta_{m0})[J_m(k_A r) + D_m H_m(k_A r)]\cos(m\theta), \tag{B1}$$

where $\delta_{m0}$ is the Kronecker symbol, $k_A$ the wave number of the matrix material, $J_m$ and $H_m$ the cylindrical Bessel and Hankel functions of the first kind, and $D_m$ the scattering coefficients. The first term in brackets corresponds to the decomposition of the incident plane wave $e^{i\vec{k}_A\cdot\vec{r}}$, and the second to the scattered amplitude.

Inside the scatterer, the acoustic pressure field is a sum of Bessel functions of the first kind $J_m$ with the associated amplitudes $B_m$:

$$p_B(r,\theta) = \sum_{m=0}^{+\infty} i^m B_m(2 - \delta_{m0}) J_m(k_B r)\cos(m\theta). \tag{B2}$$

The first boundary condition at the matrix-scatterer interface $r=R$ is the stress (or the acoustic pressure) continuity:

$$p_A(R) = p_B(R). \tag{B3}$$

The second boundary condition at $r=R$ is the normal flux continuity $(v_A)_r=(v_B)_r$, which gives, owing to the Euler relation applied to porous media [see Eq. (A2)],

$$\frac{1}{\rho_A(\omega)}\frac{\partial p_A}{\partial r}(R) = \frac{1}{\rho_B(\omega)}\frac{\partial p_B}{\partial r}(R). \tag{B4}$$

In order to find the scattering coefficients $D_m$, the expression of the acoustic pressure field Eqs. (B1) and (B2) are substituted in the two boundary conditions Eqs. (B3) and (B4). Due to the orthogonality of the $\cos(m\theta)$, the latter conditions apply separately to the different components $m$ and yield

$$D_m = \frac{\frac{Z_A}{Z_B}J_m(k_A R)J_m'(k_B R) - J_m'(k_A R)J_m(k_B R)}{H_m'(k_A R)J_m(k_B R) - \frac{Z_A}{Z_B}H_m(k_A R)J_m'(k_B R)}. \tag{B5}$$

### 2. 3D problem of spherical scatterers

In the case of spherical embedded scatterers, the analytical development is similar. The acoustic pressure field outside and inside the scatterer is written in the spherical coordinate system:

$$p_A(r,\theta) = \sum_{m=0}^{+\infty} i^m(2m + 1)[j_m(k_A r) + d_m h_m(k_A r)]P_m(\cos\,\theta), \tag{B6}$$

$$p_B(r,\theta) = \sum_{m=0}^{+\infty} i^m b_m j_m(k_B r) P_m(\cos\ \theta), \tag{B7}$$

where $j_m$ and $h_m$ are the spherical Bessel and Hankel functions of the first kind, and $P_m$ the Legendre polynomials of the first kind.

With the help of the boundary conditions Eqs. (B3) and (B4), the scattering coefficients in the 3D case are derived:

$$d_m = \frac{\frac{Z_A}{Z_B} j_m(k_A R) j'_m(k_B R) - j'_m(k_A R) j_m(k_B R)}{h'_m(k_A R) j_m(k_B R) - \frac{Z_A}{Z_B} h_m(k_A R) j'_m(k_B R)}. \tag{B8}$$

In the special case of rigid scatterers, the ratio $Z_A/Z_B$ is set to zero and the expressions (B5) and (B8) reduce to

$$D_m = -\frac{J'_m(k_A R)}{H'_m(k_A R)}, \tag{B9}$$

$$d_m = -\frac{j'_m(k_A R)}{h'_m(k_A R)}. \tag{B10}$$


[1] L. L. Foldy, Phys. Rev. **67**, 107 (1945).
[2] M. Lax, Rev. Mod. Phys. **23**, 287 (1951).
[3] P. C. Waterman and R. Truell, J. Math. Phys. **2**(4), 512 (1960).
[4] A. Ishimaru, *Wave Propagation and Scattering in Random Media* (Oxford University Press, Oxford, 1997).
[5] P. Sheng, *Introduction to Wave Scattering, Localization and Mesoscopic Phenomena* (Academic, New York, 1995).
[6] L. Tsang, J. A. Kong, and K. H. Ding, *Scattering of Electromagnetic Waves, Vol. 1: Theory and Applications* (Wiley, New York, 2000).
[7] U. Frisch, *Wave Propagation in Random Media* (Academic, New York, 1968).
[8] A. Derode, A. Tourin, and M. Fink, Phys. Rev. E **64**, 036605 (2001).
[9] J. H. Page, Ping Sheng, H. P. Schriemer, I. Jones, Xiaodun Jing, and D. A. Weitz, Science **271**, 634 (1996).
[10] R. Weaver, J. Acoust. Soc. Am. **100**(4), 2684 (1996).
[11] M. A. Biot, J. Acoust. Soc. Am. **28**, 168 (1956).
[12] M. A. Biot, J. Acoust. Soc. Am. **28**, 168 (1956).
[13] M. A. Biot, J. Appl. Phys. **33**, 1482 (1962).
[14] R. Burridge and J. B. Keller, J. Acoust. Soc. Am. **70**, 1140 (1981).
[15] D. L. Johnson, J. Koplik, and R. Dashen, J. Fluid Mech. **176**, 379 (1987).
[16] P. Sheng, Phys. Rev. B **41**, 4507 (1990).
[17] S. R. Pride, A. F. Gangi, and F. D. Morgan, J. Acoust. Soc. Am. **92**, 3278 (1992).
[18] S. R. Pride, F. D. Morgan, and A. F. Gangi, Phys. Rev. B **47**, 4964 (1993).
[19] D. Lafarge, P. Lemarinier, J.-F. Allard, and V. Tarnow, J. Acoust. Soc. Am. **102**(4), 1995 (1997).
[20] J. F. Allard, *Propagation of Sound in Porous Media: Modeling Sound Absorbing Materials* (Chapman and Hall, London, 1993).
[21] A. Cortis, D. M. J. Smeulders, J. L. Guermond, and D. Lafarge, Phys. Fluids **15**, 1766 (2003).
[22] L. D. Landau, E. M. Lifshitz, and L. P. Pitaevskii, *Electrodynamics of Continuous Media*, 2nd ed. (Pergamon, Oxford, 1984).
[23] F. Luppé, J.-M. Conoir, and H. Franklin, J. Acoust. Soc. Am. **111**(6), 2573 (2002).
[24] J. G. Berryman, J. Acoust. Soc. Am. **91**(2), 551 (1992).
[25] A. Lagendijk and B. A. Van Tiggelen, Phys. Rep. **270**, 143 (1996).
[26] P. M. Morse and K. U. Ingard, *Theoretical Acoustics* (Princeton University Press, Princeton, NJ, 1987).
[27] By definition [29], the length $\Lambda'$ is given by $2/\Lambda' = S_p/V_p$ where $V_p$ and $S_p$ are, respectively, the fluid (or pore) volume and the surface of contact between solid and fluid (or pore surface). Per unit total volume, $S_p = n2\pi R = 2f/R$ and $V_p = 1 - n\pi R^2 \simeq 1$, hence the expression given for $\Lambda'$. The expression for $\Lambda$ then expresses the relation $\Lambda = \Lambda'/2$, a result which can be shown to be valid for dilute arrays of parallel cylinders (see, e.g., Ref. [20], Appendix 5.E). The same relation may serve to derive the given $\alpha_\infty$ expression. Varying the filling ratio $f$ by means of a uniform growth of the solid phase, we may write in the first order in $f$, $\alpha_\infty = 1 + d\alpha_\infty/df|_f f$. Then using a particular "uniform growth" relation [28] Eq. (3), the derivative is found to be $\Lambda'/\Lambda - 1$, hence the result. [Notice that there is a minus sign missing in Ref. [28] Eq. (3).]
[28] D. L. Johnson, J. Koplik, and L. M. Schwartz, Phys. Rev. Lett. **57**, 2564 (1986).
[29] Y. Champoux and J.-F. Allard, J. Appl. Phys. **70**, 1975 (1991).
[30] J. G. Berryman, J. Acoust. Soc. Am. **68**, 1809 (1980); **68**, 1820 (1980).